

Exploring spatial segregation induced by competition avoidance as driving mechanism for emergent coexistence in microbial communities

Mattia Mattei ¹ and Alex Arenas ^{1,2}¹*Departament d'Enginyeria Informàtica i Matemàtiques, Universitat Rovira i Virgili, 43007 Tarragona, Spain*²*Pacific Northwest National Laboratory, 902 Battelle Boulevard, Richland, Washington 99354, USA*

(Received 22 February 2024; accepted 14 June 2024; published 8 July 2024)

This study investigates the role of spatial segregation, prompted by competition avoidance, as a key mechanism for emergent coexistence within microbial communities. Recognizing these communities as complex adaptive systems, we challenge the sufficiency of mean-field pairwise interaction models, and we consider the impact of spatial dynamics. We developed an individual-based spatial simulation depicting bacterial movement through a pattern of random walks influenced by competition avoidance, leading to the formation of spatially segregated clusters. This model was integrated with a Lotka-Volterra metapopulation framework focused on competitive interactions. Our findings reveal that spatial segregation combined with low diffusion rates and high compositional heterogeneity among patches can lead to emergent coexistence in microbial communities. This reveals a novel mechanism underpinning the formation of stable, coexisting microbe clusters, which is nonetheless incapable of promoting coexistence in the case of isolated pairs of species. This study underscores the importance of considering spatial factors in understanding the dynamics of microbial ecosystems.

DOI: [10.1103/PhysRevE.110.014404](https://doi.org/10.1103/PhysRevE.110.014404)

I. INTRODUCTION

Micro-organisms do not function in isolation; rather, they exist within multispecies communities, cohabiting the same environment and engaging in a spectrum of complex interactions. This complexity poses a substantial challenge in understanding how the physiological behaviors of individual species contribute to emergent properties such as stability, productivity, and resilience. From this perspective, microbial communities can be regarded as “*complex adaptive systems*” [1], making them well-suited for rigorous quantitative theoretical analysis. Indeed, a plethora of mathematical models have been applied to describe the microbiome. These range from variations of the Lotka-Volterra equations [2] and MacArthur’s consumer-resource model [3,4] to frameworks based on evolutionary game theory [5], among others.

Recently, Chang *et al.* [6] presented solid experimental proofs that multispecies coexistence is an *emergent phenomenon*: they isolated organisms from stable synthetic bacterial communities consisting of various species and competed all possible combination of pairs of organisms to test their ability to live together; in most cases, one species out-competed the other, leading to exclusion. From this, they concluded that coexistence in communities cannot be reduced to pairwise coexistence rules, and they left open the question about the fundamental mechanisms behind it. In particular, they wondered whether the complex nature of multispecies coexistence derives from higher-order interactions (HOIs), or whether it can be explained by a complex network of pairwise relations.

Providing a precise definition of HOIs, particularly in the field of ecology, is challenging [7]. One possible simplified conceptualization is to view HOIs as a modification

of pairwise interactions in the presence of a third or more species. The research by Mickalide and Kuehn [8] reveals a HOI aligning with this definition. An “interaction modification” unfolds, wherein a single-celled algae (*Chlamydomonas reinhardtii*) alters the dynamics between a predatory ciliate (*Tetrahymena thermophila*) and the bacterium *Escherichia coli*. This modification stems from a phenotypic change in *E. coli* triggered by the presence of *C. reinhardtii*; the algae inhibits the aggregation of *E. coli* cells, rendering them more susceptible to predation by the ciliate.

In general, it is always possible to generalize mathematical models to incorporate group interactions [9], but identifying the various and often intricate driving physical mechanisms behind them can be demanding. Before employing such sophisticated tools and concepts, we wonder whether the simpler framework of complex networks of pairwise interactions is sufficient to explain the emergent phenomena.

Studies such as those conducted by Thebault and Fontaine [10] or Rohr *et al.* [11] have illustrated how the architecture of the network of pairwise interactions among species significantly influences the stability and overall macroscopic characteristics of an ecosystem. In this context, a pertinent question emerges: why, within the same ecosystem, do certain species interact among them while others do not? Perhaps the most straightforward explanation lies in how species are *spatially distributed*.

There is abundant evidence indicating the significance of spatial constraints in the formation of microbial communities and the emergence of spatially segregated clusters of bacteria. For instance, Welch *et al.* [12] discovered highly organized spatial structure in the oral microbiome and a surprising correlation between the position in space of taxa and their function. Conwill *et al.* [13] showed how lineages with *in vitro* fitness

differences coexist within centimeter-scale regions on human skin, but each skin pore being dominated by a single lineage. Shi *et al.* [14] developed a new technology for mapping the microbiome, and they discovered that microbial communities in oral biofilms are spatially structured as stable microarchitectures over time. Cho *et al.* [15], through the utilization of an innovative microfluidic device, showed that bacterial colonies of *E. coli* have the capability to autonomously self-organize within chambers of varying shapes and sizes that permit continuous cell escape. In general, colonies of bacteria exhibit a fascinating propensity to form tight structures in various settings in response to unfavorable environmental conditions including various types of chemical stress [16].

The core concept of this study is to explore the potential of spatial self-organization among microbes as the underlying factor contributing to the observed emergent coexistence identified by Chang *et al.* To achieve this objective, it is necessary to understand bacterial movement.

Bacteria in a liquid medium exhibit a movement pattern characterized by alternating between tumble and swim phases [17]. In a uniform environment, the movement of a bacterium resembles a random walk, with relatively straight swimming segments occasionally interrupted by random tumbles that reorient the bacterium. Notably, bacteria such as *E. coli* lack the ability to deliberately choose their swimming direction and cannot maintain a straight path for an extended period due to rotational diffusion, essentially “forgetting” their trajectory. To compensate for this, they continuously assess their course and make adjustments when necessary, allowing them to steer their random walk towards favorable locations. This movement of bacteria in response to chemical gradient is called *chemotaxis*. The combination of these forces can result in complex colony formation and various types of collective motion, as proved by numerous experiments and theoretical models [18–21].

While it may be reasonable to attribute bacterial movements primarily to nutrient-driven research, it is essential to acknowledge that chemotaxis is both imprecise and energetically costly for bacteria, especially in densely populated environments (see Ref. [22]). Chemotaxis involves the ability to perceive gradients, specifically differences in nutrient concentrations across different spatial locations. In densely populated environments, discerning specific directions towards which bacteria should move becomes challenging due to the multitude of simultaneous stimuli. Additionally, when considering bacterial communities in batch cultures *in vitro*, such as those studied by Chang *et al.*, there is no clear reason to assume uneven nutrient distribution or strong nutrient gradients influencing bacterial motion. A more plausible proposition would be that the predominant driving force behind bacterial movement is an *unoriented* escape response from highly competitive environments to less competitive ones. This does not require the bacterium to calculate directions, but rather relies on sensing local density and subsequently initiating an escape. Our hypothesis is that this behavior can still be triggered even in crowded environments and may be less energetically costly compared to chemotaxis.

Following this direction, we developed an individual-based spatial simulation to depict the individual movement of bacteria, leading to the formation of spatially segregated clusters

resulting from the *escape* from regions with high competition. Under the assumption of timescale separation between movement and growth, the result of the spatial simulation was then utilized to calculate the initial conditions for a metapopulation Lotka-Volterra model with only competitive interactions, capturing the growth dynamics of such patches of bacteria. This study shows that (i) segregation of clusters of bacteria can be obtained as a result of competition avoidance only and, therefore, it can potentially occur in any conditions regardless of the environmental setup; (ii) building upon the latter justification, a metapopulation Lotka-Volterra formalism can be adopted, and this alters considerably the pattern of coexistence for the species at the equilibrium. Specifically, for low diffusion rates and high compositional heterogeneity among patches, it is possible to reproduce the emergence observed by Chang *et al.*, i.e., the formation of stable communities formed by multiple microbial species, the majority of which do not coexist when isolated in pairwise combinations. As a benchmark to validate our model, we also confirmed its ability to replicate the three macroecological laws governing microbial communities, as discovered by Grilli [23].

II. INDIVIDUAL-BASED SPATIAL SIMULATION FOR BACTERIAL MOTION

The simulation starts by uniformly distributing n bacteria within a two-dimensional square and subsequently randomly assigning each of them to one of $N < n$ different species. While other initial spatial distributions are conceivable—such as placing bacteria of the same species in closer proximity—these variations do not appear to influence the final results. Hence, we opted to proceed with the initially uniform distribution for its generality. We can then assume that each cell interacts only with the cells in its proximity. If we think about bacteria as nodes in a network, the simple formalism of a random geometric graph (RGG) [24] can be employed to rapidly evaluate the number of bacteria in the neighborhood of each node. In a RGG, two nodes are connected when their distance is within a certain neighborhood radius R . Here, the Euclidean distance is considered, i.e., two nodes i and j are connected when $d_{ij} = \sqrt{(x_i - x_j)^2 + (y_i - y_j)^2} < R$. The idea is that the higher the density of competitors in the vicinity of node i , the more it is inclined to escape from that region. Therefore, we update node positions according to

$$\begin{aligned} x_i(t+1) &= x_i(t) + I_i(t) \cos \theta_i(t), \\ y_i(t+1) &= y_i(t) + I_i(t) \sin \theta_i(t), \end{aligned} \quad (1)$$

with θ_i uniformly distributed between $[0, 2\pi]$ at each time-step, and

$$I_i(t) = \frac{R}{1 + e^{-\alpha \left(\frac{N_c^i(t)}{N_{th}} - 1 \right)}}. \quad (2)$$

Stated differently, we model bacterial movement selecting a random direction and an intensity proportional to the level of competitiveness, i.e., the number of competitors N_c^i in the neighborhood of the node i . Taking inspiration from neural networks, the intensity of motion is modeled as a sigmoid function. The parameter α controls the shape of the curve; if $\alpha \rightarrow \infty$, the function tends to the Heaviside step-function.

The threshold parameter N_{th} controls the position of the inflection point $N_c^i = N_{\text{th}}$. This function cannot be equal to zero, disallowing bacteria to be completely still, and its maximum value is equal to R , i.e., the radius of the neighborhood area. The simulation stops when all the bacteria minimize their intensity motion, i.e., when their activity results in a random walk confined in a small portion of space. Note that in this framework, there is no distinction made between different species, and all agents are considered indistinguishable at this stage. Consequently, when counting neighboring nodes, bacteria of the same species are also perceived as competitors. The underlying assumption is that, in dense environments, bacteria lack the capability (or exhibit limited efficiency) to distinguish between different species at an individual level. However, they can sense when neighboring populations become dense. If bacteria primarily perceive their environment through quorum sensing [25]—that is, by releasing signaling molecules—our hypothesis posits that in dense environments, they may respond to the overall quantity of these molecules reaching high levels, rather than identifying specific ones emitted by particular species.

To quantitatively compute the different clusters of bacteria in the final network, we employed the classical Louvain algorithm for communities detection [26]. It optimizes a quality function known as modularity, which quantifies the strength of the community structure in a network. The algorithm optimizes modularity by iteratively moving nodes between communities, enhancing the overall cohesion within communities while reducing connectivity between them. The Louvain algorithm is a popular choice in the field of network science, despite the numerous limitations associated with modularity optimization algorithms [27]. In our context, the selection of a particular algorithm has negligible effects.

We assume that the spatial rearrangement occurs rapidly enough to achieve equilibrium before species start to grow. This separation of temporal scales allows us to model growth using a classical population-based ecological model as the Lotka-Volterra formalism, adapted to our context as described in the following section.

III. METAPOPOPULATION LOTKA-VOLTERRA MODEL

The Lotka-Volterra equations are the gold standard to model the dynamics of interacting populations in ecology [28]. In the generalized version for N species, they can reproduce each possible type of relations according to the sign of the interactions matrix entries, from competition to cooperation. A growing debate surrounds the significance of positive interactions among bacterial species. Numerous studies, such as the one by Palmer and Foster [29], showed that negative interactions tend to predominate, and instances of cooperation, where two species mutually benefit, are generally infrequent. Contrary findings are presented in studies such as that of Kehe *et al.* [30], wherein positive interactions, particularly parasitisms, are identified as common occurrences, especially among strains exhibiting distinct carbon consumption profiles. In this work, we have opted for the exclusive incorporation of negative interactions in Lotka-Volterra equations. We posit that the simpler and more justified assumption lies in considering competition for nutrients as the primary

environmental-mediated interactions shaping bacterial populations.

Given that the initial setup involves spatially separated bacterial clusters, adopting a metapopulation model proves advantageous. Metapopulation models are frameworks in ecology that conceptualize the dynamics of interconnected populations within a fragmented landscape. Coined by Levins [31], the metapopulation concept views a population as a set of subpopulations occupying discrete patches of habitat, with occasional migration or dispersal occurring between these patches. The dynamics of each subpopulation are influenced by local factors such as birth, death, and interactions, as well as the exchange of individuals among patches. Ngoc *et al.* offer an illustration of the Lotka-Volterra formalism tailored for metapopulation in their work [32]. Their model explores the dynamics of two species in competition for an implicit resource within a habitat divided into two patches.

In this work, we have adapted the Lotka-Volterra formalism as follows:

$$\begin{aligned} \frac{dX_{i\alpha}(t)}{dt} = & r_i X_{i\alpha}(t) \left(1 - \frac{1}{K_\alpha} \sum_{j \in \alpha} A_{ij} X_{j\alpha}(t) \right) \\ & + \mu \sum_{\beta}^{N_p} M_{\alpha\beta} (X_{i\beta}(t) - X_{i\alpha}(t)), \end{aligned} \quad (3)$$

where the Latin indices refer to species, while the Greek ones refer to the different N_p patches; thus, $X_{i\alpha}$ represents the population of species i in patch α . The intrinsic growth rate of species i is indicated as r_i and the carrying capacity with K_α . Note that the latter depends on the patch rather than on the species. This aligns with our spatial simulation, where a patch is characterized by the maximum bacterial density that does not trigger the escape response. For the same reason, we will assume that each patch has the same carrying capacity, denoted as $K_\alpha = K$, for all patches. The interaction coefficient A_{ij} depends only on the species types i and j , and the sum in the first term runs over all the species j placed in patch α , i.e., species interact only if in the same patch. Moreover, in this formulation the entries of \mathbf{A} are all positive in order to reproduce only competitive interactions. The final term, modulated by the coefficient μ , incorporates diffusion when, for example, a species grows enough to spread to neighboring patches. The matrix \mathbf{M} represents the network connecting the patches, obtained from the last random geometric graph provided by the simulation. In particular, $M_{\alpha\beta} = m_{\alpha\beta}/n_\alpha n_\beta$, with $m_{\alpha\beta}$ the number of links between the communities, and n_α, n_β the number of nodes in α and β , respectively. In summary, the weights $M_{\alpha\beta}$ quantify the spatial proximity between different patches.

A. Stability of Lotka-Volterra equations

As μ approaches 0, the equilibrium solutions within each patch become well-established and are solely dependent on the interaction pattern and carrying capacities, given by $X_{i\alpha}^* = \sum_{j \in \alpha} (\mathbf{A}^{-1})_{ij} K$. It is recognized that for global stability of the feasible fixed point ($X_{i\alpha}^* > 0 \ \forall i, \alpha$), the matrix \mathbf{A} must be negative-definite. In other words, $\mathbf{A} + \mathbf{A}^T$ should possess exclusively negative eigenvalues, as thoroughly explained by

Grilli *et al.* in their study [33]. In his groundbreaking research [34], May demonstrated that large ecological networks exhibit a notably low probability of stability. Specifically, when matrix entries are sampled from a random distribution with a mean of zero and a mean square value of α , the system is almost certain to be unstable if $\alpha > 1/\sqrt{N}$. Building upon May's findings, Allesina and Tang [35] extended the results differentiating between the various types of relationships, including predator-prey, competition, or mutualism. They provided analytical stability criteria for each scenario. The key takeaway from these insights is that in the case of competition, system stability is only assured when there is a predominant presence of very weak interactions.

Mathematical analyses of stability typically focus on conditions near equilibrium points due to analytical challenges in dealing with nonlinear systems at a distance from equilibrium. For this reason, Holling [36] suggested defining the behavior of ecological systems with two distinct properties: resilience and stability. Resilience pertains to the persistence of relationships within a system and measures its ability to absorb changes in state variables, driving variables, and parameters while still persisting. Stability, on the other hand, refers to a system's capacity to return to equilibrium after a temporary disturbance, with a more rapid and less fluctuating return indicating greater stability. The well-known *mutual invasion criterion*, often associated with the concept of resilience, serves as a notable benchmark. For stable coexistence, it demands that each species within a community demonstrates positive population growth rates when invading a preexisting community of competitors from low density [37]. This is exactly the indicator used by Chang *et al.* to assess stable coexistence in their experimental communities of microbial species. Take a moment to focus on a scenario involving only two species within the system. In the context of competitive Lotka-Volterra equations with identical carrying capacities, it is established that the invasion criterion holds true when both A_{12} and A_{21} are less than 1 [38]. Consequently, note that weak interactions with zero mean would almost always satisfy the invasion criterion and, consequently, lead to stable coexistence. However, Chang *et al.* [6] observed in their experiments that only a relatively small fraction (about 30%) of possible pairs of species complies with the invasion criterion. When contemplating the parameters A_{ij} as "universal" coefficients for pairwise interactions, i.e., only depending on species' types, it appears that these experimental results are scarcely consistent with the conditions necessary for mathematical asymptotic stability. The work by Abramson and Zanette [39] provides us with a workaround. They randomly selected interaction coefficients for a system comprising N Lotka-Volterra species from a uniform distribution centered around one. Remarkably, the resulting phase space exhibited a multitude of fixed points, with a majority featuring both positive and negative eigenvalues—indicating instability. Consequently, the system traverses various unstable equilibria, leading to instances in which the population of certain species undergoes pseudoextinctions, reaching very low concentrations before rebounding. The noteworthy finding in their study is the demonstration that introducing a lower bound, X_0 , to the populations induces a shift in the stability of nearly all equilibria, transforming them into stable states.

All of these heuristic discussions provide compelling justifications for our parameter choices in the model, which will be detailed in Sec. IV. Moreover, we recall that our theoretical setup incorporates the structural aspect of patches, a factor that significantly influences coexistence and stability requirements. The next section will provide further clarification on this point.

B. Mesoscopic interpretation of the interactions parameters

Let us consider the dynamics for the entire population $X_i = \sum_{\alpha} X_{i\alpha}$ of the species rather than focusing on the subpopulations in individual patches. If we express the population of species i in terms of fractions ϕ ranging from 0 to 1 [i.e., $X_{i\alpha}(t) = \phi_{i\alpha}(t)X_i(t)$], we obtain the following equation:

$$\frac{dX_i(t)}{dt} = r_i X_i(t) \left(1 - \frac{1}{K} \sum_{\alpha, j} \phi_{i\alpha}(t) A_{ij} \phi_{j\alpha}(t) X_j(t) + \frac{\mu}{r_i} \sum_{\alpha, \beta} M_{\alpha\beta} [\phi_{i\beta}(t) - \phi_{i\alpha}(t)] \right). \quad (4)$$

Because the metapopulation network is undirected, i.e., $M_{\alpha\beta} = M_{\beta\alpha}$, the last term of the above equation is zero. Indeed, the migration between patches does not affect the global population. To recover the standard Lotka-Volterra equations for entire populations, we define

$$A_{ij}^G(t) \equiv A_{ij} S_{ij}(t) = A_{ij} \sum_{\alpha} \phi_{i\alpha}(t) \phi_{j\alpha}(t). \quad (5)$$

Here, S_{ij} , ranging between 0 and 1, measures the *proximity* between species i and j , i.e., the extent of segregation between them, indicating how much they occupy the same patches. When they do not share any patches, S_{ij} is zero; when their entire populations are in the same patch, $S_{ij} = 1$. This interpretation of the global interaction parameters A_{ij}^G combines the "true" strength of interaction A_{ij} between two species with the mesoscale spatial distribution across patches. It is noteworthy that even two strongly interacting species with a high A_{ij} can have a limited global impact on each other if they are adequately segregated in space. Indeed, the proximity measure changes the solutions at equilibrium, which now have to satisfy

$$\sum_j (\mathbf{S}^* \odot \mathbf{A})_{ij} X_j^* = K. \quad (6)$$

Let us see how the invasion criterion in the case of two species changes in this new fashion. Suppose that species 1 is rare, $X_1 \sim 0$, while species 2 is at equilibrium, X_2^* :

$$\begin{aligned} \frac{dX_2^*}{dt} &= r_2 X_2^* \left(1 - \frac{1}{K} \sum_{\alpha} (\phi_{2\alpha}^*)^2 A_{22} X_2^* \right) \\ &= 0 \Leftrightarrow X_2^* = \frac{K}{A_{22} \sum_{\alpha} (\phi_{2\alpha}^*)^2}. \end{aligned} \quad (7)$$

Species 1 will be able to invade the system if $dX_1(t)/dt > 0$, i.e., if

$$A_{12} < \frac{\sum_{\alpha} (\phi_{2\alpha}^*)^2}{\sum_{\alpha} \phi_{1\alpha} \phi_{2\alpha}^*} \equiv \Omega_{21}, \quad (8)$$

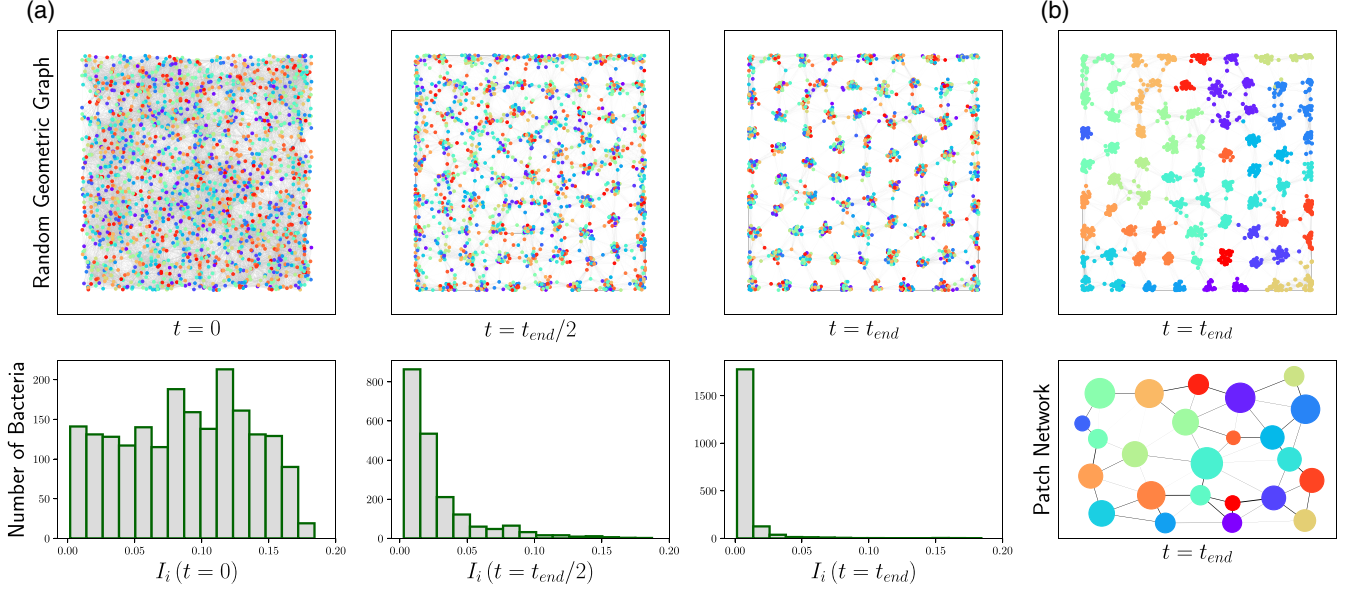


FIG. 1. In this example, the individual-based simulation was conducted in a two-dimensional square of dimensions 2×2 with $R = 0.2$, $\alpha = 7$, and $N_{\text{th}} = 60$. We considered $n = 2000$ nodes (bacteria) randomly assigned to $N = 100$ different species. The top row of panel (a) presents the random geometric network representation of the system where each species is indicated with a different color, while the bottom row illustrates the intensity motion distribution as described by Eq. (2), both shown at three different time-steps ($t = 0$, $t = t_{\text{end}}/2$ and at the end of the simulation t_{end}). In panel (b), we present the outcome of the community detection algorithm. Initially, we depict the identified communities using distinct colors (top row). Subsequently, we construct a patch network wherein communities are represented by individual nodes of corresponding colors (bottom row). In this network, the size of each node is proportional to the number of bacteria within the community, and the edges are weighted based on the number of links connecting the communities.

where we have considered $A_{ii} = 1$. To comply with the mutual invasion criterion, the same must hold also for A_{21} , inverting the indices. However, species 2, in the absence of species 1, has grown equally in all the patches until equilibrium; this means that $\phi_{2\alpha}^* = 1/N_p$, $\forall \alpha$. Considering also that $\sum_{\alpha} \phi_{1\alpha} = 1$, we obtain that the factor Ω is equal to 1 and we revert to the classical invasion criterion conditions. This elucidates how the mesoscale structure can at the same time relevantly affect the global interactions A_{ij}^G , and so the steady state, for species in communities while maintaining the same conditions for pairwise stable coexistence in the sense of the invasion criterion.

C. Macroecological laws

A recent contribution by Grilli [9] represents a significant stride in the macroecological exploration of microbial communities. Through the analysis of data from different biomes, the study delineates patterns of abundance variation, encapsulating three macroecological laws: (i) the abundance fluctuations of any given species across samples adhere to a γ distribution; (ii) the variances of these distributions for distinct species are proportional to the square of their means, known as Taylor's law [40]; and (iii) the mean abundances across species conform to a log-normal distribution. He also showed how a stochastic logistic model (SLM), which enhances a logistic growth with a multiplicative stochastic term reproducing environmental effects, can perfectly reproduce the phenomenology. In an even more recent work by Camacho-Mateu *et al.* [41], a generalized stochastic Lotka-Volterra model (SLVM) was introduced, incorporating pairwise interactions. This model was also able to uphold Grilli's three

empirical laws. They considered only weak interactions in order to comply with the global stability of the feasible fixed point requirements. We will demonstrate that our framework can replicate Grilli's laws, even when accounting for stronger interactions and incorporating information about environmental stochasticity within our spatial simulation.

IV. RESULTS

We conducted multiple runs of our spatial simulation, considering $n = 2000$ bacteria, i.e., nodes in the RGG, assigned to $N = 100$ different species and exploring various values of the radius R and threshold N_{th} . Remarkably, for each radius value, it is always possible to find a corresponding N_{th} such that the simulation reaches a form of equilibrium relatively quickly. This equilibrium comprises different spatially segregated clusters of bacteria, where each bacterium attains a very low velocity of motion and predominantly occupies a single patch. Figure 1 presents an example of a simulation with $R = 0.2$, $\alpha = 7$, and $N_{\text{th}} = 60$, with snapshots of the system at different time-steps. In panel (a) the RGG is displayed alongside the associated intensity motion distribution. As the nodes cluster, the distribution shifts towards very low values. This phenomenon persists across all the higher values of R investigated, extending up to 0.5. The straightforward outcome of increasing the distance in the RGG is a reduction in the number of patches and an increase in their dimensions. Consequently, for the subsequent analysis, we focus solely on the case in which $R = 0.2$. This specific value arises as the lowest threshold at which a patchy network forms within a relatively short time frame. Lower values resulted in bacteria

interacting with an insufficient number of neighboring individuals, leading to rapid attainment of equilibrium without the formation of a patch structure. Conversely, higher values delayed equilibrium to an unacceptable extent, as we assume that these processes occur before the initiation of species growth.

All the simulations are performed in a 2×2 bidimensional square. It is important to note that the range of velocities considered is biologically plausible: bacteria can move at a wide range of speeds ranging from 1 to 1000 $\mu\text{m/s}$ [42]; considering the square as $2 \times 2 \text{ mm}^2$, this implies that bacteria at the beginning of our simulation travel on average 141 μm in a few seconds of straight-line motion, with a maximum possible value of about 280 μm ; then, at the end of simulation, they all reach velocities of very few μm per second.

Upon reaching equilibrium, each simulation yields the initial distribution of various species across patches, representing the initial conditions in our metapopulation model for species growth. We normalized the resulting discrete abundances for the total population of each patch and then we numerically solved the system of differential equations using an explicit Runge-Kutta method of order 5. For simplicity, we opted for identical and unitary intrinsic growth rates and carrying capacities for all patches and species ($K_\alpha = 1$, $\forall \alpha$, $r_i = 1$, $\forall i$). In light of Sec. III A, we chose not to require asymptotic stability but to follow a direction similar to Abramson *et al.* [39], therefore we randomly sampled the off-diagonal entries of the interaction matrix from a log-normal distribution with a mean (ν) set to 1, varying its variance (σ^2) from 0.05 to 0.5 [$A_{ij} \sim \text{log-normal}(\nu, \sigma)$]. The diagonal elements were uniformly set to 1 ($A_{ii} = 1$). Additionally, we incorporated a lower limit for the population, denoted as $X_{i\alpha}^0$, set at 10^{-3} . Furthermore, we explored various values for the diffusion parameter (μ), spanning from 0 to 1. Confirming the findings of Abramson *et al.* [39], in this setup we observed that the numerical simulations display equilibrium. We considered the system to exhibit equilibrium dynamics if the coefficient of variation for the populations of the species was below 1% in the last 500 time-steps. This criterion was met in the majority of cases, while in some instances, species' populations exhibited oscillatory behavior. We focused solely on the former cases for our analysis. To assess the stability of these equilibrium configurations, we employ the mutual invasion criterion. This involves systematically reducing the abundance of each surviving species at equilibrium one by one and observing whether they exhibit a positive growth rate, ultimately returning to values close to their previous abundance levels (note that this perturbation occurs abruptly and does not allow the system to reequilibrate). We observed that approximately 90% of the surviving species consistently demonstrate regrowth potential in all the cases investigated, guaranteeing a form of stability for our simulated systems. Those species that became extinct were primarily those with already minimal abundance levels at equilibrium.

The idea is to organize the simulations to replicate the procedure in [6]: the spatial simulation ends up with the RGG at equilibrium, on which we employed the modularity optimization Louvain algorithm which successfully identifies distinct communities, i.e. the different patches of the metapopulation network [panel (b) of Fig. 1]. Afterwards, we use the

metapopulation Lotka-Volterra formalism to simulate species growth and to identify the species that reach equilibrium. Subsequently, we proceed to reexecute the entire model again, including both spatial simulation and growth, considering all the possible pairs of survivors. Consistent with the experimental design, we investigate three different initial distribution proportions for the pairs (50%-50%, 95%-5%, 5%-95%) to assess their potential for coexistence under each scenario in the absence of the other species.

The initial series of simulations consisted of 100 runs, considering different combinations of the interaction standard deviation (σ) along with the diffusion parameter (μ). We examined three values of σ (0.05, 0.1, and 0.5) and three values of μ (0.1, 0.3, and 0.5). Figure 2 displays the outcomes for the number of survivors (N_S) while varying σ and keeping μ constant (top row), and vice versa (bottom row). A vertical dashed red line indicates the mean number of surviving species over 100 runs of the classical mean-field Lotka-Volterra without patch structure. Notably, across all cases, the patch structure consistently facilitates a significantly higher number of surviving species compared to the mean-field scenario, indicative of enhanced coexistence among species. The distribution shifts towards higher values for the number of survivors with higher σ and lower diffusion rates μ . This latter trend can be explained straightforwardly: as μ increases, species can explore the entire patch network more rapidly, converging towards the classical mean-field approach. Conversely, when variance increases, the distribution exhibits heavier tails, and the correlation between higher variances and a greater number of survivors suggests that increased heterogeneity in the interaction patterns among species, and therefore in the composition of the patches, can promote coexistence. We will revisit the effect of heterogeneity later in our analysis.

Further insights can be obtained looking to the fractions ϕ_i before and after executing the model. Specifically, refer to Fig. 3 to observe the ‘‘proximity measure’’ S_{ij} , as defined in Eq. (5), for each pair of species both before and after allowing them to grow and migrate. In the initial state, S_{ij} exhibits a bell-shaped distribution, indicating that the spatial simulation results in species that are, on average, evenly segregated among the patches. Following the model execution, the surviving species demonstrate a distribution more concentrated around zero and with a long tail, suggesting that survivors are more likely to be highly segregated with a small minority of them being able to coexist in the same patches. As described by Eq. (5), this phenomenon facilitates the coexistence of species, even when their net interaction A_{ij} is high. This last analysis suggests that the mechanism behind the observed multispecies coexistence is that the majority of patches are dominated by a single species (or just few of them) who, due to strong interaction coefficients, cannot be invaded or invade neighboring patches. In this scenario, the initial distribution of species and the specific structure of the metapopulation network become crucial factors, as further explored in the next two analyses.

First, we aim to assess the influence of the initial distribution of species across the patches on the number of coexisting species at equilibrium. To achieve this, rather than conducting our spatial simulation, we sampled the initial populations from a Dirichlet distribution to ensure equal abundances for

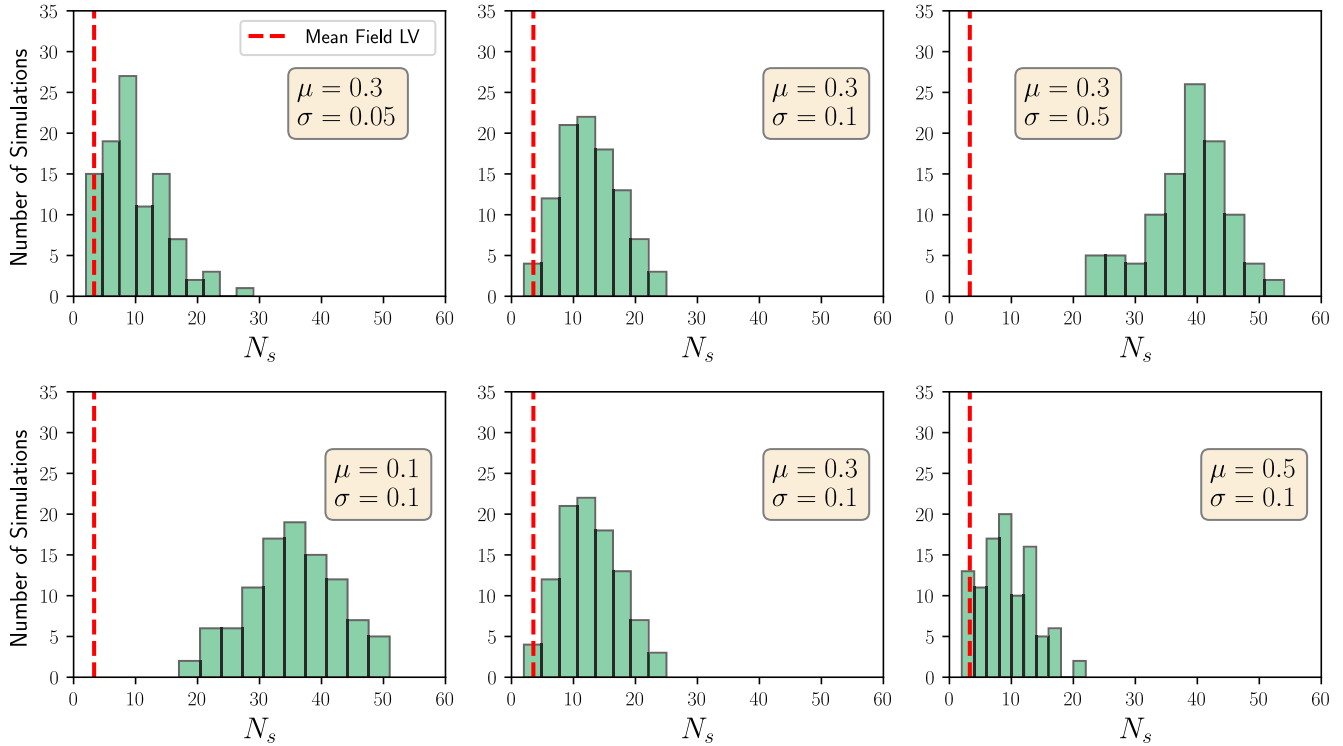


FIG. 2. Distributions of the number of survivors (N_s) obtained after 100 runs of the spatial simulation and the metapopulation model for three different values of the interaction standard deviation $\sigma = 0.05, 0.1, 0.5$, while keeping $\mu = 0.3$ in the top row and for $\mu = 0.1, 0.5, 0.5$ while keeping $\sigma = 0.1$ in the bottom one. The vertical dashed red line indicates the mean number of surviving species over 100 runs of the classical mean-field Lotka-Volterra model (mean-field LV). For all the simulations $n = 2000, N = 100, R = 0.2, N_{th} = 60, \alpha = 7, K_\alpha = 1$, and $r_i = 1 \forall i, X_{i\alpha}^0 = 10^{-3} \forall (i, \alpha)$.

all species [$\sum_{\alpha=1}^{N_p} X_{i\alpha}(0) = 1$], but with varied distributions among the patches,

$$\vec{X}_i(0) = (X_{i1}(0), X_{i2}(0), \dots, X_{iN_p}(0)), \quad (9)$$

$$p(\vec{X}_i(0)) = \frac{1}{\mathcal{N}} \prod_{\alpha=1}^{N_p} X_{i\alpha}^{a_\alpha - 1}(0), \quad (10)$$

with \mathcal{N} the normalization factor (multivariate beta function) and $\vec{a} = (a_1, \dots, a_{N_p})$ concentration parameters for the

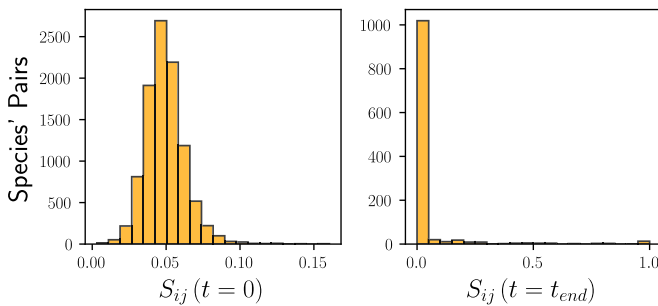


FIG. 3. Distribution of the proximity measure S_{ij} , as defined in Eq. (5), for each possible pair of species, before and after species' growth and over 100 runs of the complete model. Given that S_{ij} is not defined when one or both species are extinct, in the final state we considered all possible couples of only survived species. For the simulation here, $n = 2000, N = 100, R = 0.2, N_{th} = 60, \alpha = 7, \sigma = 0.1, \mu = 0.3, K_\alpha = 1$ and $r_i = 1 \forall i, X_{i\alpha}^0 = 10^{-3} \forall (i, \alpha)$.

different patches. We chose to consider equal $a_\alpha = a, \forall \alpha$, in order to give the same importance to all the patches. Lowering the global parameter a introduces greater random variability in the species' concentration among the patches, and therefore higher heterogeneity in the patch composition. We conducted multiple model runs, varying the value of a from 100 to 0.01 while simultaneously adjusting the diffusion rate to generate the heat map depicted in Fig. 4. The figure highlights that lower values of the diffusion rate and greater variability between patch compositions (lower a) yield the best performance in terms of the number of surviving species. This further suggests that heterogeneity promotes coexistence among multiple species. Upon attempting to describe the initial distribution of species yielded by our spatial simulation with the Dirichlet distribution, we find that the value of a which best fits it is approximately 0.1 (indicated by the dashed horizontal line in Fig. 4). This indicates that the spatial simulation effectively reproduces highly heterogeneous patches.

Another intriguing aspect to consider is the role of the patch network in reproducing the observed coexisting patterns. To investigate this, we conducted multiple simulations, examining three distinct network types characterized by varying levels of connectivity. Here, connectivity refers to a fraction between 0 and 1, representing the number of realized links divided by the maximum possible number of edges $n(n-1)/2$ for a given set of nodes n . We examined the following three networks types (Fig. 5): (i) The Newman-Watts-Strogatz graph [43], resembling a grid where each node maintains a fixed number of connections but also allows

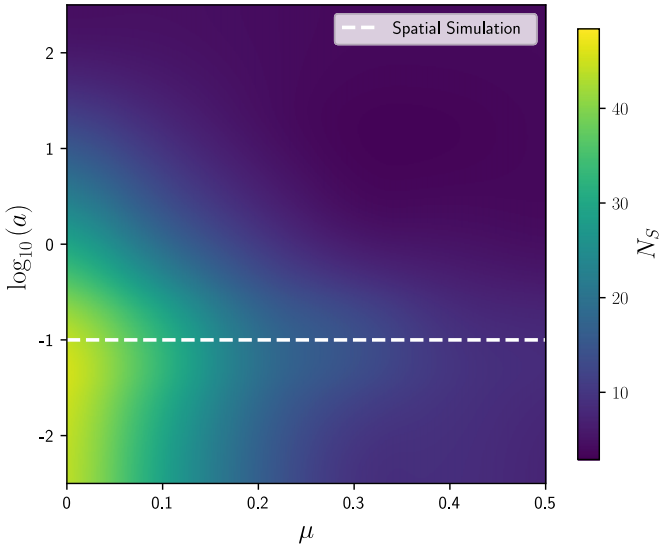


FIG. 4. The heat map depicts the number of survivors (N_S) at the equilibrium varying the initial distribution of the species, through the concentration parameter a in a Dirichlet distribution (y-axis in log scale), and the diffusion rate μ (x-axis). Brighter colors indicate higher values for the number of survivors. The white horizontal dashed line indicates the value of a which best fits with the initial distribution of the species provided by our spatial simulation. For each pair of values (a, μ) we performed 100 runs of the model with $\sigma = 0.1$, $K_\alpha = 1$ and $r_i = 1 \forall i$, $X_{i\alpha}^0 = 10^{-3} \forall (i, \alpha)$. To ensure the figure appears continuous, we used quadratic interpolation.

for additional shortcuts between non-neighboring nodes; (ii) the Erdos-Renyi graph [44], representing a standard random network where links are randomly established based on a pre-determined probability; and (iii) a “Mainland-type” network [45], featuring a single central patch connected to all others, with options to include extra links between peripheral patches to control connectivity. Across all three network types, we conducted 100 simulations of the model, considering four different levels of connectivity for each while keeping other model features fixed. It is evident that the network structure primarily influences the results through its connectivity, with an increase in connectivity correlating with a decrease in the number of coexisting species at equilibrium across all network types. Evaluating the effect of different topologies at the same level of connectivity is less straightforward. However, it appears that the specific structure also plays a role, particularly evident at lower connectivity levels, where the three types exhibit more distinct distributions. The last two analyses conducted demonstrate how compositional heterogeneity of the initial conditions and sparseness in the metapopulation network promote coexistence at equilibrium; both of these features are reproduced by our spatial simulation, which now, under this perspective, becomes essential to explain the results at equilibrium.

Interestingly enough, upon reexecuting the model for all possible pairs of surviving species after all simulations, we discovered that only a minority of pairs can coexist in isolation, mirroring the experimental findings and replicating the emergent behavior. The boxplot in Fig. 6 illustrates the distributions of the percentage of species’ pairs coexisting

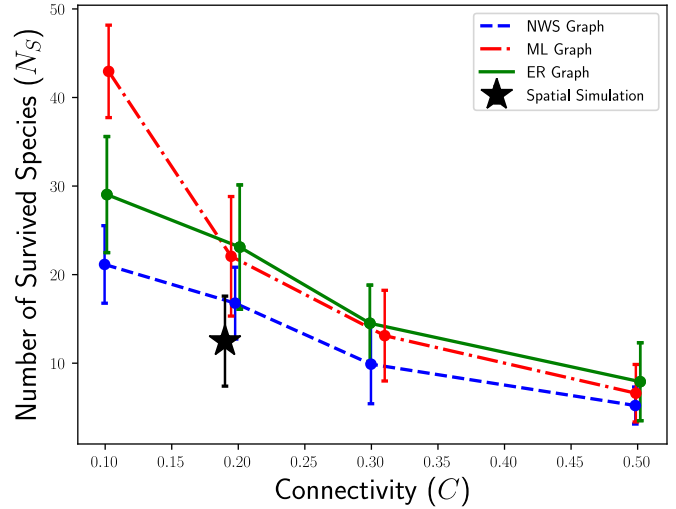


FIG. 5. This graph illustrates how the number of coexisting species at equilibrium is influenced by the connectivity of the patch network across three different topologies. Points here are averages over 100 simulations of the metapopulation model for four different connectivity values and for all three network types. The Newman-Watts-Strogatz (NWS) graph, denoted with a dashed blue line, features nodes with a fixed degree and the possibility of additional shortcuts. The Mainland network (ML), depicted with a dashed-dotted red line, consists of a central main patch connected to all others, with additional links between the latter with varying probabilities. Results for the Erdos-Renyi graph (ER), where nodes are randomly connected based on a fixed probability, are displayed with a solid green line. The star marker indicates the mean connectivity and number of survived species provided by the model when the metapopulation network emerges from the spatial simulation. Other parameters of the model were held constant, with $\sigma = 0.1$, $\mu = 0.3$, $K_\alpha = 1$, $\forall \alpha$, $r_i = 1$, $\forall i$, and $X_{i\alpha}^0 = 10^{-3}$ for all combinations of species i and patches α .

in isolation for the same combinations of μ and σ as previously examined. A horizontal dashed line represents the value reported by [6], which stands at 28.5%. Specifically, cases with the highest σ and the lowest μ demonstrate a significantly high probability of replicating the experimental value. For the remaining cases, although the average probabilities exceed those observed experimentally, again only a minority of pairs exhibit coexistence. In fact, in the absence of multiple species, spatial self-organization in this scenario leads to a random process distributing both species equally across all patches with high probability. This implies an unaffected interaction pattern, rendering the spatial distribution incapable of promoting coexistence, in contrast to what happens in the case of multiple species, where the spatial simulation naturally generates more heterogeneous patches. When there is a significant disparity in the initial concentration of the two species, as previously mentioned, the patch structure does not impact the invasion criterion when one species invades the other. Consequently, the mesoscale structure, while potentially influencing coexistence in multispecies configurations, does not change the criteria for coexistence in the case of two species. This elucidates the findings illustrated in Fig. 6.

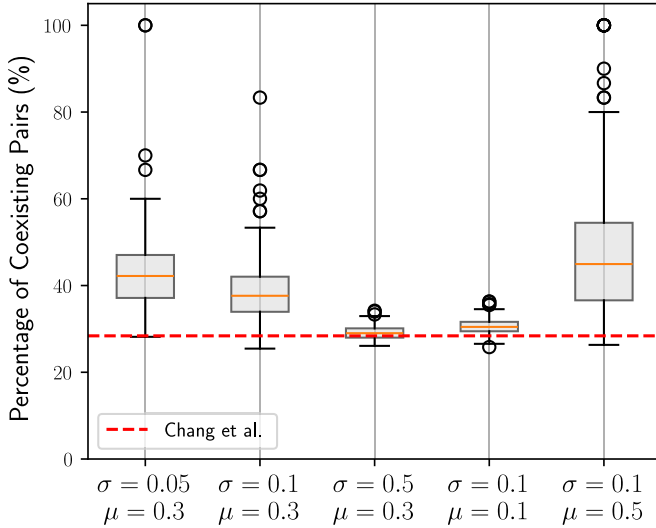


FIG. 6. Each box represents the distribution for the percentage of coexisting species' pairs (picked from the set of survivors in the multispecies simulation) over 100 runs for different combinations of μ and σ , as depicted along the x -axis. The box extends from the first quartile (Q1) to the third quartile (Q3) of the data, with a line at the median. The whiskers extend from the box to the farthest data point lying within $1.5 \times$ the interquartile range (IQR) from the box. Flier points indicate outliers. The red horizontal dashed line indicates the experimental value for the percentage of coexisting pairs found in [6]. For the multispecies part, the chosen parameters are $n = 2000$, $N = 100$, $R = 0.2$, $N_{\text{th}} = 60$, $K_{\alpha} = 1$, and $r_i = 1 \forall i$, $X_{i\alpha}^0 = 10^{-3} \forall (i, \alpha)$. The same for the two-species part except for $N = 2$.

As mentioned earlier, a robust testing ground for a model aspiring to describe the microbiome involves verifying its ability to replicate the three macroecological laws outlined in Sec. III C. To achieve this, we conducted 100 model runs, again for different combinations of the interactions variance and the diffusion rate, and then we checked for the abundance distribution of species across samples [abundance fluctuation distribution (AFD)], the relationship between the variance and mean of species abundances, and the distribution of mean abundances across species [mean abundance distribution (MAD)]. In the left column of Fig. 7 the three laws are displayed, considering σ fixed to 0.1 and for three different values of $\mu = 0.1, 0.3, 0.5$. In the right column we did the same but fixing μ to 0.3 and for three values of $\sigma = 0.05, 0.1, 0.5$. The three laws are depicted along the rows. All these analyses demonstrated good agreement with the patterns identified by Grilli, resulting in mean R^2 values of 0.97, 0.5, and 0.86, respectively, for the three laws. The fits are performed considering a number of bins of the distributions for the first and the third law according to the Freedman-Diaconis rule [46].

Note that our exploration of the agreement of the AFD to a γ distribution was conducted only at the aggregate level while in [23] it was observed also at species level. Due to our specific choice of interactions, the majority of species become extinct in each simulation run, and those that survive vary across different runs. As a result, statistical data for most species may not adequately explore the entire γ distribution at

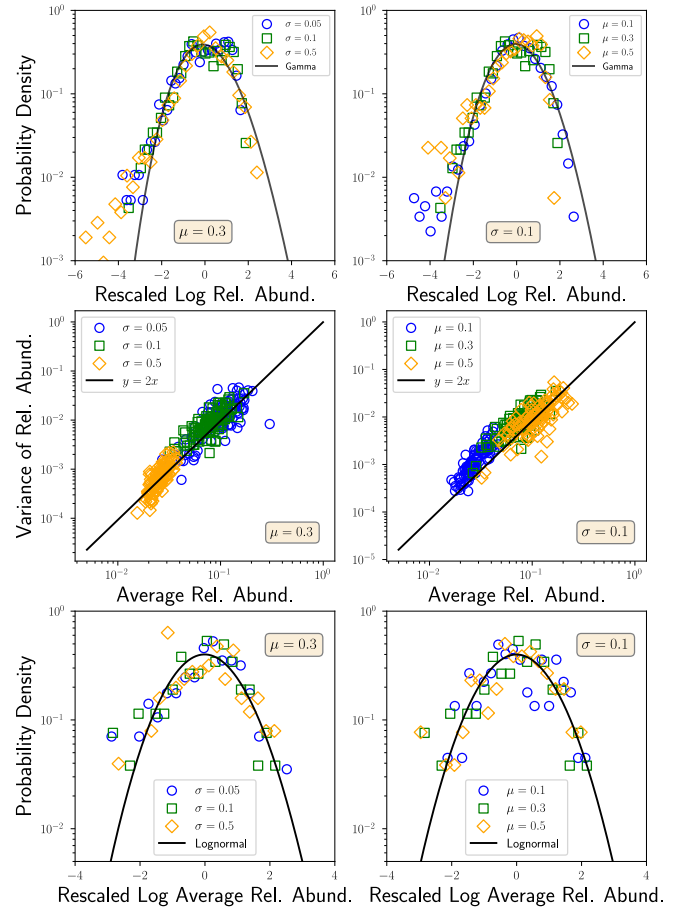


FIG. 7. The simulations were conducted with $\sigma = 0.1$ and varying μ across 0.1, 0.3, and 0.5 for the plots in the right column. Similarly, the simulations were repeated with $\mu = 0.3$ while adjusting σ to 0.05, 0.1, and 0.5 in the left column. The different colors of the circles represent the three values of μ in the right column and of σ in the left column. The remaining parameters in the model were set as in Fig. 2. The top row presents the abundance fluctuation distribution, depicting the probability density for the rescaled log relative abundance of the species across 100 model runs. Here, the black line represents a γ distribution. In the second row, we plotted the variance of the relative abundance as a function of the corresponding means across 100 simulations. The black line corresponds to Taylor's law with an exponent of 2. The third row displays the distribution for the rescaled log average relative abundance, again across 100 different simulations, compared with a log-normal distribution (black line). The analysis yielded mean R^2 values of 0.97, 0.5, and 0.86, respectively, for the three laws.

the individual species level, and aggregation may yield better results.

The second law exhibits less alignment with theoretical expectations. Nevertheless, recent findings [47] strongly indicate that the second law cannot be regarded as a precise relationship between mean and variance. Instead, the exponent appears to be sampled from a distribution rather than remaining a constant, leading to increased dispersion in data points, as observed in our case. This hypothesis finds support in both empirical observations and the predictions of an approximate theory.

In the context of the stochastic logistic model, achieving a log-normal MAD involves sampling carrying capacities from a log-normal distribution. In our study, the emergence of this pattern appears to be linked to the log-normally distributed interactions. To investigate further, we conducted a brief analysis where interactions were sampled from a normal distribution with a mean of 1 and varying variances (0.1, 0.3, and 0.5). Interestingly, in this revised setup, the MAD deviated further from a log-normal distribution compared to the previous case (Euclidean distance decreased by one-half and the R -squared value decreased by one-third).

V. DISCUSSION

In this study, we have developed a theoretical framework that combines an individual-based spatial simulation of bacterial motion with a metapopulation Lotka-Volterra model to describe abundance dynamics. The current model has demonstrated its capability to replicate certain experimental phenomena, such as the intriguing emergence of coexistence observed by Chang *et al.* Specifically, the model facilitates coexistence in multispecies systems by fostering the spatial rearrangement of bacteria into distinct clusters. This spatial segregation is a consequence of a high escape response triggered when the local environment becomes densely populated and competitive. The self-organization into different patches consistently leads to a greater number of bacteria surviving, as spatial separation limits interactions among them. However, this process proves to be less efficient in the case of a two-species system. When two species have a strong interaction, the only viable way to coexist is complete segregation within the system. If bacteria are uniformly distributed, there is a high probability that both species will end up in each patch, therefore not changing the pattern of competition. In summary, our spatial simulation demonstrates the capability to generate heterogeneous patches in scenarios involving multiple species, whereas this heterogeneity is not observed in cases with only two isolated species. This discrepancy results in the promotion of coexistence in the former case, while not in the latter.

The exploration of how a spatial structure influences the outcomes of a standard Lotka-Volterra model has been previously examined in the literature. As stated by Denk and Hallatschek [48], several theoretical studies [49,50] on metacommunities and metapopulations have repeatedly shown that dispersal between patches can alleviate global extinctions of species and stabilize biodiversity, whereas we illustrated how increasing the diffusion parameter leads to more extinctions. We believe that this apparent discrepancy can be attributed to the choice of interaction regime. All these studies primarily explored the weak regime ($\nu \ll 1$), while we investigate the area bordering niche partitioning ($\nu < 1$) and competitive exclusion ($\nu > 1$). In their case, species survival hinges on local species extinction being balanced by dispersal from within the metacommunity. In contrast, in our scenario, diffusion merely enhances connectivity among strongly interacting species, thereby reducing coexistence.

One could posit that the described phenomenon occurs because bacteria, when assessing the density of surrounding competitors, are unable to discriminate between different species. This leads to the inclusion of cells from the same

species as perceived competitors. However, there is no inherent reason to assume any form of cooperation between bacteria of the same species. As mentioned earlier, cooperation, although possible, tends to be infrequent both among bacteria of the same species and across different species [29,51,52]. This rationale underlies our decision to exclusively consider negative interactions in the formulation of the growth model.

Similarly, it can be argued that the absence of uneven nutrient distribution in our model may impose limitations on its applicability. Nevertheless, when considering experimental communities, they are typically cultured in agar plates or batch cultures where nutrients are generally thoroughly mixed, resulting in a uniform distribution throughout the medium. Given this context, we assume that there is no substantial nutrient concentration gradient influencing bacterial motion. Thus, we posit that the predominant driving force for movement is the avoidance of competition, and we showed how even in isotropic environments with no particular nutrient distribution, is still possible to have a spatial structure with metacommunities affecting the coexistence among species. A consumer-resource model would necessitate making various assumptions about nutrient abundances, types, temporal dynamics, spatial distribution, and more. The Lotka-Volterra formalism allows the modeling of resource competition without delving into specific resource details.

Bacteria rank among the fastest reproducers globally, doubling at the scale of minutes [53]. However, their motion is also remarkably rapid, with swimming speeds exceeding 100 body lengths per second [54,55]. This substantiates our assumption of effectively separating the temporal scales between self-organization in space and growth.

While numerous instances of empirical evidence support bacterial self-organization in space, our model currently lacks experimental validation. Nevertheless, we have shown that our theoretical framework aligns with the three macroecological laws identified by Grilli, providing a form of empirical confirmation. Efforts are underway to experimentally validate our assumptions and to scale the model for increased biological plausibility. Future endeavors will involve a significantly higher number of bacteria situated in a three-dimensional space with varied geometry, a task currently beyond reach due to the limits of the computational power at our disposal.

In conclusion, we believe that our approach is innovative as it validates the utilization of population-based models integrating mesoscale structures. While a fully microscopic approach poses technical challenges, a mean-field approach would oversimplify, and existing works incorporating mesostructures often do not provide generative mechanisms for them. We introduced a microscopic process that potentially rationalizes the adoption of patch configurations. Simultaneously, we illustrated how minimal adaptability levels can lead to the formation of isolated bacterial clusters, maintaining a high degree of randomness that mirrors the intricate stimuli influencing bacterial motion. We believe that this work has the potential to pave the way for a new research direction, emphasizing the importance of considering the delicate spatial equilibrium between species within a microbial community as a pivotal element to be incorporated into theoretical models and investigations.

ACKNOWLEDGMENTS

This project has received funding from the European Union's Horizon 2020 research and innovation programme under the Marie Skłodowska-Curie Grant Agreement No. 945413 and from the Universitat Rovira i Virgili (URV). A.A. acknowledge support from Spanish Ministerio de Ciencia e Innovacion (No. PID2021-128005NB-C21), Generalitat de Catalunya (No. 2021SGR-633 and No. PDAD14/20/00001), and Universitat Rovira i Virgili (No. 2019PFR-URV-B2-41), support from ICREA Academia, and the James S. McDonnell Foundation (220020325), the

European Union's Horizon Europe Programme under the CREXDATA project, Grant Agreement No. 101092749 and the Joint Appointment Program at Pacific Northwest National Laboratory (PNNL). PNNL is a multi-program national laboratory operated for the U.S. Department of Energy (DOE) by Battelle Memorial Institute under Contract No. DE-AC05-76RL01830.

A.A. and M.M. designed the study; M.M. performed simulations, mathematical calculations, and data analysis; A.A. supervised the results; A.A. and M.M. wrote and approved the manuscript.

The authors declare no conflict of interest.

-
- [1] H.-S. Song, W. R. Cannon, A. S. Beliaev, and A. Konopka, Mathematical modeling of microbial community dynamics: A methodological review, *Processes* **2**, 711 (2014).
- [2] K. Z. Coyte, J. Schluter, and K. R. Foster, The ecology of the microbiome: Networks, competition, and stability, *Science* **350**, 663 (2015).
- [3] J. E. Goldford, N. Lu, D. Bajić, S. Estrela, M. Tikhonov, A. Sanchez-Gorostiaga, D. Segrè, P. Mehta, and A. Sanchez, Emergent simplicity in microbial community assembly, *Science* **361**, 469 (2018).
- [4] A. Posfai, T. Taillefumier, and N. S. Wingreen, Metabolic trade-offs promote diversity in a model ecosystem, *Phys. Rev. Lett.* **118**, 028103 (2017).
- [5] E. Frey, Evolutionary game theory: Theoretical concepts and applications to microbial communities, *Physica A* **389**, 4265 (2010).
- [6] C.-Y. Chang, D. Bajić, J. C. C. Vila, S. Estrela, and A. Sanchez, Emergent coexistence in multispecies microbial communities, *Science* **381**, 343 (2023).
- [7] A. Sanchez, Defining higher-order interactions in synthetic ecology: Lessons from physics and quantitative genetics, *Cell Syst.* **9**, 519 (2019).
- [8] H. Mickalide and S. Kuehn, Higher-order interaction between species inhibits bacterial invasion of a phototroph-predator microbial community, *Cell Syst.* **9**, 521 (2019).
- [9] J. Grilli, G. Barabás, and M. Michalska-Smith *et al.*, Higher-order interactions stabilize dynamics in competitive network models, *Nature (London)* **548**, 210 (2017).
- [10] E. Thébault and C. Fontaine, Stability of ecological communities and the architecture of mutualistic and trophic networks, *Science* **329**, 853 (2010).
- [11] R. P. Rohr, S. Saavedra, and J. Bascompte, On the structural stability of mutualistic systems, *Science* **345**, 1253497 (2014).
- [12] J. L. M. Welch, B. J. Rossetti, C. W. Rieken, F. E. Dewhirst, and G. G. Borisy, Biogeography of a human oral microbiome at the micron scale, *Proc. Natl. Acad. Sci. USA* **113**, 10807 (2016).
- [13] A. Conwill, A. C. Kuan, and R. Damerla *et al.*, Anatomy promotes neutral coexistence of strains in the human skin microbiome, *Cell Host. Microbe* **30**, 171 (2022).
- [14] H. Shi, Q. Shi, and B. Grodner *et al.*, Highly multiplexed spatial mapping of microbial communities, *Nature (London)* **588**, 676 (2020).
- [15] H. J. Cho, H. Jönsson, K. Campbell, P. Melke, J. W. Williams, B. Jedynak, A. M. Stevens, A. Groisman, and A. Levchenko, Self-organization in high-density bacterial colonies: Efficient crowd control, *PLOS Biol.* **5**, e302 (2007).
- [16] L. Hall-Stoodley, J. Costerton, and P. Stoodley, Bacterial biofilms: from the natural environment to infectious diseases, *Nat. Rev. Microbiol.* **2**, 95 (2004).
- [17] H. Berg and D. Brown, Chemotaxis in escherichia coli analysed by three-dimensional tracking, *Nature (London)* **239**, 500?504 (1972).
- [18] A. Czirók, E. Ben-Jacob, I. Cohen, and T. Vicsek, Formation of complex bacterial colonies via self-generated vortices, *Phys. Rev. E* **54**, 1791 (1996).
- [19] M. S. Alber, M. A. Kiskowski, and Y. Jiang, Two-stage aggregate formation via streams in myxobacteria, *Phys. Rev. Lett.* **93**, 068102 (2004).
- [20] X. L. Wu and A. Libchaber, Particle diffusion in a quasi-two-dimensional bacterial bath, *Phys. Rev. Lett.* **84**, 3017 (2000).
- [21] F. Peruani, J. Starruß, V. Jakovljevic, L. Søgaaard-Andersen, A. Deutsch, and M. Bär, Collective motion and nonequilibrium cluster formation in colonies of gliding bacteria, *Phys. Rev. Lett.* **108**, 098102 (2012).
- [22] D. R. Brumley, F. Carrara, A. M. Hein, Y. Yawata, S. A. Levin, and R. Stocker, Bacteria push the limits of chemotactic precision to navigate dynamic chemical gradients, *Proc. Natl. Acad. Sci. USA* **116**, 10792 (2019).
- [23] J. Grilli, Macroecological laws describe variation and diversity in microbial communities, *Nat. Commun.* **11**, 4743 (2020).
- [24] M. Penrose, *Random Geometric Graphs*, Oxford Studies in Probability (Oxford Academic, Oxford, 2003).
- [25] S. Mukherjee and B. L. Bassler, Bacterial quorum sensing in complex and dynamically changing environments, *Nat. Rev. Microbiol.* **17**, 371?382 (2019).
- [26] V. D. Blondel, J.-L. Guillaume, R. Lambiotte, and E. Lefebvre, Fast unfolding of communities in large networks, *J. Stat. Mech.* (2008) P10008.
- [27] T. P. Peixoto, Hierarchical block structures and high-resolution model selection in large networks, *Phys. Rev. X* **4**, 011047 (2014).
- [28] V. Volterra, Variations and fluctuations of the number of individuals in animal species living together, *ICES J. Marine Sci.* **3**, 3 (1928).
- [29] J. D. Palmer and K. R. Foster, Bacterial species rarely work together, *Science* **376**, 581 (2022).

- [30] J. Kehe, A. Ortiz, A. Kulesa, J. Gore, P. C. Blainey, and J. Friedman, Positive interactions are common among culturable bacteria, *Sci. Adv.* **7**, eabi7159 (2021).
- [31] R. Levins, Some demographic and genetic consequences of environmental heterogeneity for biological control, *Bull. Entomol. Soc. Am.* **15**, 237 (1969).
- [32] D. Nguyen Ngoc, R. B. de la Parra, M. A. Zavala, and P. Auger, Competition and species coexistence in a metapopulation model: Can fast asymmetric migration reverse the outcome of competition in a homogeneous environment? *J. Theor. Biol.* **266**, 256 (2010).
- [33] J. Grilli, M. Adorisio, and S. Suweis *et al.*, Feasibility and coexistence of large ecological communities, *Nat. Commun.* **8**, 14389 (2017).
- [34] R. May, Will a large complex system be stable? *Nature (London)* **238**, 413 (1972).
- [35] S. Allesina and S. Tang, Stability criteria for complex ecosystems, *Nature (London)* **483**, 205 (2012).
- [36] C. S. Holling, Resilience and stability of ecological systems, *Annu. Rev. Ecol. Syst.* **4**, 1 (1973).
- [37] T. N. Grainger, J. M. Levine, and B. Gilbert, The invasion criterion: A common currency for ecological research, *Trends Ecol. Evol.* **34**, 925 (2019).
- [38] R. MacArthur and R. Levins, The limiting similarity, convergence, and divergence of coexisting species, *Am. Naturalist* **101**, 377 (1967).
- [39] G. Abramson and D. H. Zanette, Statistics of extinction and survival in lotka-volterra systems, *Phys. Rev. E* **57**, 4572 (1998).
- [40] L. Taylor, Aggregation, variance and the mean, *Nature (London)* **189**, 732 (1961).
- [41] J. Camacho-Mateu, A. Lampo, M. Sireci, M. Á. Muñoz, and J. A. Cuesta, Sparse species interactions reproduce abundance correlation patterns in microbial communities, *Proc. Natl. Acad. Sci. USA* **121**, e2309575121 (2024).
- [42] H. C. Berg, The rotary motor of bacterial flagella, *Annu. Rev. Biochem.* **72**, 19 (2003).
- [43] M. E. J. Newman and D. J. Watts, Renormalization group analysis of the small-world network model, *Phys. Lett. A* **263**, 341 (1999).
- [44] P. Erdős and A. Rényi, On random graphs, *Publ. Math. Debrecen* **6**, 290 (1959).
- [45] R. H. MacArthur and E. O. Wilson, *The Theory of Island Biogeography* (Princeton University Press, Princeton, NJ, 1967).
- [46] D. Freedman and P. Diaconis, On the histogram as a density estimator: L_2 theory, *Z. Wahrscheinlichkeit. Ver. Geb.* **57**, 453 (1981).
- [47] J. Camacho-Mateu, A. Lampo, S. Ares, and J. A. Cuesta, Non-equilibrium microbial dynamics unveil a new macroecological pattern beyond Taylor's Law, [arXiv:2404.07090](https://arxiv.org/abs/2404.07090).
- [48] J. Denk and O. Hallatschek, Self-consistent dispersal puts tight constraints on the spatiotemporal organization of species-rich metacommunities, *Proc. Natl. Acad. Sci. USA* **119**, e2200390119 (2022).
- [49] D. Gravel, F. Massol, and M. Leibold, Stability and complexity in model meta-ecosystems, *Nat. Commun.* **7**, 12457 (2016).
- [50] M. T. Pearce, A. Agarwala, and D. S. Fisher, Stabilization of extensive fine-scale diversity by ecologically driven spatiotemporal chaos, *Proc. Natl. Acad. Sci. USA* **117**, 14572 (2020).
- [51] M. E. Hibbing, C. Fuqua, M. R. Parsek, and S. B. Peterson, Bacterial competition: surviving and thriving in the microbial jungle, *Nat. Rev. Microbiol.* **8**, 15 (2010).
- [52] K. R. Foster and T. Bell, Competition, not cooperation, dominates interactions among culturable microbial species, *Curr. Biol.* **22**, 1845 (2012).
- [53] R. J. Allen and B. Waclaw, Bacterial growth: a statistical physicist's guide, *Rep. Prog. Phys.* **82**, 016601 (2019).
- [54] J. G. Mitchell, L. Pearson, and S. Dillon, Clustering of marine bacteria in seawater enrichments, *Appl. Environ. Microbiol.* **62**, 3716 (1996).
- [55] R. H. Luchsinger, B. Bergersen, and J. G. Mitchell, Bacterial swimming strategies and turbulence, *Biophys. J.* **77**, 2377 (1999).